

Development of Instantaneous Temperature Imaging in Sooty Flames

Doctoral Dissertation

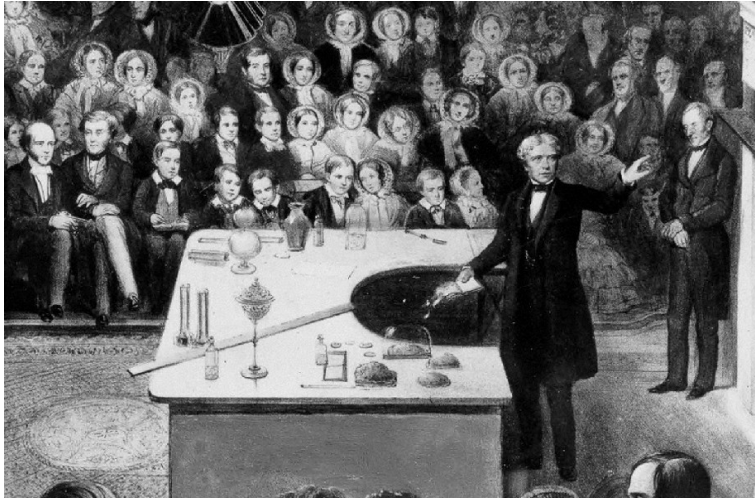
Qing N. Chan

January 2011



School of Chemical Engineering
Faculty of Engineering, Mathematical and Computer Sciences
The University of Adelaide, Australia

This page intentionally left blank.



**“It is to this presence of solid particles in the candle-flame that it owes its
brilliancy.”**

Michael Faraday

19th century British Physicist

This page intentionally left blank.

Declarations

This work contains no material that has been accepted for the award of any other degree or diploma in any university or other tertiary institution and, to the best of my knowledge and belief, contains no material previously published or written by another person, except where due reference has been made in the text.

I give consent to this copy of my thesis when deposited in the University Library, being made available for loan and photocopying, subject to the provisions of the Copyright Act 1968.

The author acknowledges that copyright of published works arising from this thesis (as listed in Appendix C) resides with the copyright holder(s) of those works.

I also give permission for the digital version of my thesis to be made available on the web, via the University's digital research repository, the Library catalogue, the Australasian Digital Theses Program (ADTP) and also through web search engines, unless permission has been granted by the University to restrict access for a period of time.

Qing N. Chan

This page intentionally left blank.

Acknowledgements

This work would not have been possible without the invaluable contributions and support from numerous people. First and foremost, I must acknowledge the reliable supervision and outstanding assistance provided by my academic supervisors, Dr Zeyad Alwahabi, Prof. Gus Nathan, A/Prof. Bassam Dally and Dr Paul Medwell, whose tutelage has guided me through the highs and lows of a research student. In particular, I owe my deepest gratitude to Dr Paul Medwell, who has made available his support in many ways. It is also necessary for me to thank Dr Peter Kalt, for his insights on work-related and not-so-work-related matters.

I am also indebted to many of the staff members from both Chemical and Mechanical Engineering Departments. In particular, I would like to thank Mary Barrow, Elaine Minerds, Wendy Brown and Yvette Knapp from the offices; Andrew Wright, the Chemical Engineering School's safety officer; Sahn Tran and Billy Constantine, from the IT support group; Richard Pateman, Jason Peak and Jeffrey Hiorns from the workshops, for their constant support throughout the course of this work.

I am also grateful towards my friends, particularly Lucy Lu, Adrian Wun, Tran Nguyen, Winnie Wong, Phuc Nguyen, Ivan Ho, Melissa Supangat and Ryan Tan, for their support and companionship. Above all, I must express my gratitude towards my family for their endless support. Without them, none of this would have been possible.

This page intentionally left blank.

Abstract

This dissertation reports on the single-shot temperature imaging in sooty flames, based on the development of two-line atomic fluorescence (TLAF), with neutral Indium atom as seeded thermometry species. The TLAF technique in the linear excitation regime has previously been demonstrated to be feasible in sooty environments but single-shot imaging, which requires a higher signal-to-noise ratio (SNR), has been elusive.

The previous TLAF theory has been extended from the linear excitation into the nonlinear excitation fluence regime. Nonlinear regime two-line atomic fluorescence (NTLAF) provides superior signal, and improves single-shot precision from ~ 250 K for the linear TLAF to ~ 100 K for the NTLAF. The NTLAF technique is shown to resolve the temperature profiles across a range of equivalence ratios for natural gas, hydrogen, and ethylene laminar premixed flames, with deviation from radiation-corrected thermocouple measurements not exceeding 100 K, and typically ~ 30 K. Measurements in lightly sooty flames demonstrate good capacity of the NTLAF technique to exclude interferences that hamper most two-dimensional laser-based thermometry techniques.

The developed technique has been further assessed in a laminar nonpremixed flame. The results show the expediency of the technique in the study of the reaction zone, and reveal interesting findings about the Indium formation process. The temperature profile across the reaction zone shows good agreement with laminar flame calculations. Indium fluorescence is observed to be strongest at the flame front, where the temperature exceeds 1000 K.

Indium has been typically seeded into flame as Indium Chloride dissolved in distilled water. The feasibility to improve on the signal quality of the developed

technique, through the substitution of distilled water with an organic solvent (namely acetone, isopropanol, methanol, and ethanol) as the seeding solution, has been examined. Acetone and methanol are shown to enhance the fluorescence signal intensity the most (approximately threefold to fivefold at stoichiometric flame condition) when used. Acetone and methanol are also shown to improve the fluorescence emission across a range of equivalence ratios, most significantly in the rich combustion region, as well as a twofold enhancement in the SNR. The use of acetone or methanol, has the potential to reduce the precision of the measurements down to ~ 60 K.

The use of the NTLAF technique for measurements in flames with high soot loadings was assessed. In particular, the interferences from soot or its precursors on the fluorescence measurements have been evaluated. The findings indicate that interferences, such as spurious scattering and laser-induced incandescence (LII), from soot are not significant. However, interferences from soot precursors, predominantly condensed species (CS) and perhaps polycyclic aromatic hydrocarbons (PAH), are substantial. Potential detection schemes to correct or circumvent these interferences have been identified.

The technical feasibility of the NTLAF technique to be used concurrently with the LII technique to provide simultaneous single-shot imaging of temperature and soot concentration has been demonstrated. The joint NTLAF-LII method has been applied to laminar premixed and nonpremixed flames, as well as a wrinkled nonpremixed flame. No significant interference of the two measurement techniques on each other is observed, for the detection and timing schemes employed. The images also reveal that, whilst NTLAF has a limited operating range, this range is sufficient to span all regions with soot. This observation demonstrates the applicability of the joint NTLAF-LII method in assessing the coupled dependency of temperature and soot in flame.

Contents

Declarations	i
Acknowledgements	iii
Abstract	v
1 Introduction	1
1.1 Motivation	1
1.2 Aims	5
1.3 Dissertation Layout	5
2 Background Literature	9
2.1 Laser Diagnostics in Sooty Flames	9
2.2 Laser-Based Thermometry Techniques	10
2.3 Two-Line Atomic Fluorescence	15
2.4 Laser-Based Soot Measurement Techniques	19
3 Experimental Details	21
3.1 Burners and Seeding Arrangements	21
3.2 Laser Systems	29
3.3 Experimental Layout	30
3.4 Data Processing	36
3.5 General Error Sources	38

4	Linear Two-Line Atomic Fluorescence (TLAF)	43
4.1	Introduction	43
4.2	Methodology	44
4.3	Experimental Arrangement	45
4.4	Results and Discussion	47
4.5	Summary	55
5	Assessment of Nonlinear Regime TLAF (NTLAF) in Laminar Premixed Flames	57
5.1	Introduction	57
5.2	Methodology	58
5.3	Experimental Arrangement	59
5.4	Results and Discussion	61
5.5	Summary	69
6	Assessment of NTLAF in Laminar Nonpremixed Flames	71
6.1	Introduction	71
6.2	Experimental Arrangement	72
6.3	Results and Discussion	73
6.4	Summary	77
7	Solvent Effects on NTLAF Measurements	79
7.1	Introduction	79
7.2	Methodology	80
7.3	Experimental Arrangement	82
7.4	Results and Discussion	83
7.5	Summary	93
8	Application of NTLAF in Sooty Flames	95
8.1	Introduction	95

8.2	Experimental Arrangement	96
8.3	Results and Discussion	100
8.4	Summary	114
9	Simultaneous Application of NTLAF and LII	115
9.1	Introduction	115
9.2	Experimental Arrangement	116
9.3	Results and Discussion	118
9.4	Summary	125
10	Summary and Conclusions	127
A	Theoretical Derivations	151
A.1	Linear Two-Line Atomic Fluorescence	151
A.2	Nonlinear Two-Line Atomic Fluorescence	153
B	Radiation Correction	155
C	Publications	157

This page intentionally left blank.

List of Figures

2.1	The relative distribution of the irradiated laser line, the Rayleigh line and the transmission curve of the iodine filter as a function of wavenumber.	11
2.2	CARS excitation diagram of a N ₂ molecule.	12
2.3	Schematic diagram of the fluorescence processes for Indium. . . .	17
2.4	Well-characterized calibration flames employed for the calibration of LII measurements.	20
3.1	Photograph of the square flat-flame burner and the premixed flame, here firing natural gas.	23
3.2	Cutaway view of the square flat-flame burner.	23
3.3	Photograph of the circular flat flame burner with a honeycomb matrix.	24
3.4	Cutaway view of the circular flat-flame burner.	24
3.5	Photograph of the JHC burner.	26
3.6	Cutaway view of the JHC burner.	26
3.7	Photograph of the pneumatic nebulizer.	28
3.8	Photograph of the ultrasonic nebulizer.	28
3.9	Pictorial representation of experimental layout.	30
3.10	Schematic details of experimental layout.	32
3.11	Timing details for the lasers and the detection systems for simultaneous TLAF/LII.	33
3.12	Timing diagram for simultaneous TLAF/LII.	34
3.13	General data processing steps.	37

4.1	Energy transitions involved in the TLAF process.	44
4.2	Indium fluorescence as a function of spectral intensity in the linear fluence regime. The fluorescence signals are normalized to the local maximum values.	47
4.3	Indium fluorescence as a function of Indium Chloride concentration. The fluorescence signals are normalized to the local maximum values.	48
4.4	Typical instantaneous images of (a) Stokes, (b) anti-Stokes Indium fluorescence and (c) temperature in Flame 1 (Table 4.1).	51
4.5	Typical averaged images of (a) Stokes, (b) anti-Stokes Indium fluorescence and (c) deduced temperature in Flame 1 (Table 4.1).	53
4.6	Typical deduced 200-shot averaged temperature image in Flame 2 (Table 4.1).	54
4.7	Indium fluorescence as a function of spectral intensity to the maximum achievable laser fluence.	55
5.1	Flame fluorescence as a function of tank fluorescence for (a) Stokes and (b) anti-Stokes processes. Dots: NTLAF measurements. Solid line: curve fit.	60
5.2	Typical instantaneous images of (a) Stokes and (b) anti-Stokes Indium fluorescence and (c) deduced temperature in Flame 1 (Table 5.1).	62
5.3	Temperature histograms for a typical instantaneous image of Flame 1 (Table 5.1) for (a) linear ($2500 \text{ W/cm}^2/\text{cm}^{-1}$) and (b) nonlinear ($250,000 \text{ W/cm}^2/\text{cm}^{-1}$) excitation regimes.	63
5.4	Normalized fluorescence signal in Flame 3 (Table 5.1) as a function of equivalence ratio. The fluorescence signals are normalized with respect to the local maximums.	64
5.5	Temperature of Flame 3 (Table 5.1) over a range of equivalence ratios for NTLAF and calibrated thermocouple measurements.	65
5.6	Temperature of Flame 4 (Table 5.1) over a range of equivalence ratios for NTLAF and calibrated thermocouple measurements.	66
5.7	Temperature of Flame 5 (Table 5.1) over a range of equivalence ratios for NTLAF and calibrated thermocouple measurements.	67

5.8	(a) Photograph of natural light emission from ethylene/air flame with $\Phi=2.25$ showing soot. Dashed area indicates approximately laser-imaging area. (b) Instantaneous NTLAF temperature image for this flame with nonlinear fluence excitation ($250,000 \text{ W/cm}^2/\text{cm}^{-1}$).	68
6.1	Typical instantaneous images of (a) Stokes and (b) anti-Stokes fluorescence and (c) deduced temperature in a laminar nonpremixed flame.	74
6.2	Boltzmann fraction as a function of temperature.	75
6.3	Temperature profile across the reaction zone of a laminar nonpremixed flame, from NTLAF measurements and laminar flame calculations.	76
7.1	Typical instantaneous images of (a) Stokes and (b) anti-Stokes fluorescence in a laminar premixed natural gas flat-flame.	84
7.2	Normalized Indium Stokes and anti-Stokes fluorescence for five different seeding solutions for a flame equivalence ratio of 1.0. The fluorescence signals are normalized with respect to the fluorescence signal recorded with water as seeding solution.	85
7.3	Normalized Indium (a) Stokes and (b) anti-Stokes fluorescence over a range of concentration of organic solvents within seeding solution, balanced with water. The fluorescence signals are normalized by the fluorescence recorded with water as seeding solution.	87
7.4	Indium fluorescence as a function of flame equivalence ratio.	88
7.5	Normalized fluorescence signal as a function of flame equivalence ratio. The fluorescence signals are normalized with respect to local maximums.	90
7.6	Relative gain in SNR of the Indium fluorescence as a function of flame equivalence ratio.	91
7.7	Temperature histograms from typical instantaneous images of laminar premixed flame with a flame equivalence ratio of ~ 1.55 with (a) acetone (b) methanol and (c) water as seeding solution.	92
8.1	Typical averaged on-wavelength (a) Stokes, (b) anti-Stokes measurements and (c) LII soot volume fraction distribution in Flame 2 (Table 8.1).	99

8.2	Typical averaged off-wavelength (a) Stokes and (b) anti-Stokes measurements in Flame 2 (Table 8.1).	100
8.3	Typical averaged on-wavelength measurements, with off-wavelength measurements overlaid for (a) Stokes and (b) anti-Stokes processes in Flame 2 (Table 8.1).	102
8.4	Typical averaged off-wavelength measurements with LII soot volume fraction overlaid for (a) Stokes and (b) anti-Stokes processes in Flame 2 (Table 8.1).	102
8.5	Average radial profiles for the (a) Stokes and (b) anti-Stokes processes extracted at a HAB of 25 mm in Flame 2 (Table 8.1).	104
8.6	Averaged radial profiles for the on-wavelength measurements at four different laser fluences, extracted at a HAB of 25 mm in Flame 2 (Table 8.1).	106
8.7	Maximum off-wavelength to on-wavelength measurements ratio as a function of laser fluence.	107
8.8	Averaged radial profiles as a function of radial distance from peak soot volume fraction location, extracted at a HAB of 25 mm in Flame 1 to 5 (Table 8.1).	109
8.9	Averaged radial profiles for the corrected on-wavelength measurements at four different laser fluences, extracted at a HAB of 25 mm in Flame 2 (Table 8.1).	111
8.10	Averaged radial profiles extracted at a HAB of 25mm in Flame 1 (Table 8.1).	112
8.11	Comparison of the maximum off-wavelength to on-wavelength measurements ratio and the maximum soot volume fraction at different flame equivalence ratios.	113
9.1	Simultaneous single-shot images for a laminar premixed ethylene-air flame. (a) Stokes, (b) anti-Stokes Indium fluorescence, (c) NTLAF temperature and (d) LII soot volume fraction.	120
9.2	Simultaneous single-shot images for a laminar nonpremixed ethylene-air flame. (a) Stokes, (b) anti-Stokes Indium fluorescence, (c) NTLAF temperature, (d) LII soot volume fraction and (e) instantaneous temperature field with location of soot overlaid (in grey).	123

9.3	Simultaneous single-shot images of a wrinkled nonpremixed ethylene-air flame. (a) Stokes, (b) anti-Stokes Indium fluorescence, (c) NTLAF temperature, (d) LII soot volume fraction and (e) instantaneous temperature field with location of soot overlaid (in grey).	124
9.4	Soot volume fraction as a function of temperature for laminar nonpremixed and wrinkled nonpremixed flames.	125

This page intentionally left blank.

List of Tables

4.1	Premixed flat-flame conditions.	46
4.2	Maximum temperature measurements and calculations for a pre-mixed natural gas/air flame.	50
5.1	Premixed flat-flame conditions.	61
7.1	Premixed flat-flame conditions.	82
7.2	Selected physical properties of the solvents at 20 °C and 1 atm, and the median diameters of the resultant droplets estimated using Lang's correlation.	82
8.1	Parameters of the fuel stream at the exit of the central fuel jet, issuing into a fixed air co-flow, for the flame conditions of interest.	97

This page intentionally left blank.